Landau-Zener transition rates of superconducting qubits and the absorption spectrum in quantum dots

Jorge G. Russo [1,2,*] and Miguel Tierz [3,†]

[1] *Institució Catalana de Recerca i Estudis Avançats (ICREA), Passeig de Lluis Companys, 23, 08010 Barcelona, Spain*

[2] *Departament de Física Cuántica i Astrofísica and Institut de Ciències del Cosmos, Universitat de Barcelona, Martí Franquès, 1, 08028 Barcelona, Spain*

[3] *Departamento de Análisis Matemático y Matemática Aplicada, Universidad Complutense de Madrid, 28040 Madrid, Spain*

(Received 13 November 2023; accepted 20 February 2024; published 4 March 2024)

Exact formulas are derived for systems involving Landau-Zener transition rates and for absorption spectra in quantum dots. These rectify previous inaccurate approximations utilized in experimental studies. The exact formulas give an explicit expression for the maxima and minima of the transition rate at any oscillating period and reveal a number of striking physical consequences, such as the suppression of oscillations for half-integer values of the detuning parameter and that the periodic dependence on the detuning parameter changes at special values of the driving field amplitude. The fluorescence spectra of quantum dots exhibit similar properties.

DOI: 10.1103/PhysRevA.109.033702

I. INTRODUCTION

The production of a coherent superposition between quantum states in nanoelectronic circuits is one of the cornerstones for the development of quantum technology [1]. A distinguished example of this is Landau-Zener-Stückelberg-Majorana (LZSM) interferometry [2,3], which formerly was also simply known as Landau-Zener interferometry. The LZSM theory, first developed in the context of the study of spin dynamics and slow atomic collisions, demonstrated that transitions are possible between two approaching levels as a control parameter is swept across the point of minimum energy splitting. (For a detailed account of all the different aspects and nuances of the first four seminal contributions, see [3–6].)

In LZSM interferometry, a quantum two-level system is driven strongly across an avoided energy-level crossing producing first a quantum superposition between the two states of the system. The temporal evolution of the two states occurs with different dynamical phases and, after a second passage through the anticrossing, coherent interference between these two states occurs. A periodically driven field can also induce coherent Rabi oscillations for a different regime of parameters. Rabi oscillations occur when the driving frequency $\nu = \omega/2\pi$ is of the same order as the energy-level separation $\Delta E/\hbar$. The rate-equation-based description, where transitions occur through the Landau-Zener effect, arises at $\hbar\nu \ll \Delta E$ and strong driving amplitude $A \sim \Delta E$ (for discussions, see [3,7]).

There is an analogy between LZSM interferometry and Mach-Zehnder interferometry since the beam splitters can be realized by Landau-Zener (LZ) transitions at a level avoided crossing and, over one oscillation period of the driving field, the qubit is swept through the avoided crossing twice. This point of view was developed in, for example, [3,8] and it is applicable to settings discussed below, such as the double-passage setting (which is related to optical Mach-Zehnder interferometry [3]).

Landau-Zener-Stückelberg-Majorana interferometry has been studied in a number of platforms. In the first part of this paper, we will be focusing on works where the platform is based on superconducting Josephson junctions [7,9] (see also [10]). These works are characterized by the presence of noise, but Landau-Zener transitions in externally driven systems have been considered, for example, also under dissipation [11,12] and in the context of other mesoscopic systems [13].

We will thoroughly reanalyze the transition rate in [7,9], providing an exact analytical expression for it as well as an improved asymptotic characterization of the rate, which will include a more accurate portrayal of the oscillations with full analytical control.

The mathematical formula describing the LZSM transition rate also appears in the study of the absorption spectrum of quantum dots, with a reinterpretation of the parameters. In the second part we will examine settings involving various external fields. An example consists in a system describing the dipole coupling of the quantum dot to a laser field. Concretely, we consider InAs/GaAs quantum dots (nanoscale islands of InAs embedded in a GaAs matrix) as studied in [14] and study the absorption spectrum for two different configurations.

We will also study the two-level system with modulated laser light discussed in [15], which appeared prior to the discovery of quantum dots, but it is nevertheless governed by related physics. Finally, we will examine the power spectrum of quantum dots in the presence of a bichromatic electromagnetic field, investigated in [16], which is expressed as an infinite series of Mollow triplets [17]. Here the corresponding infinite sums will be computed analytically.

*jorge.russo@icrea.cat
†mtierz@ucm.es

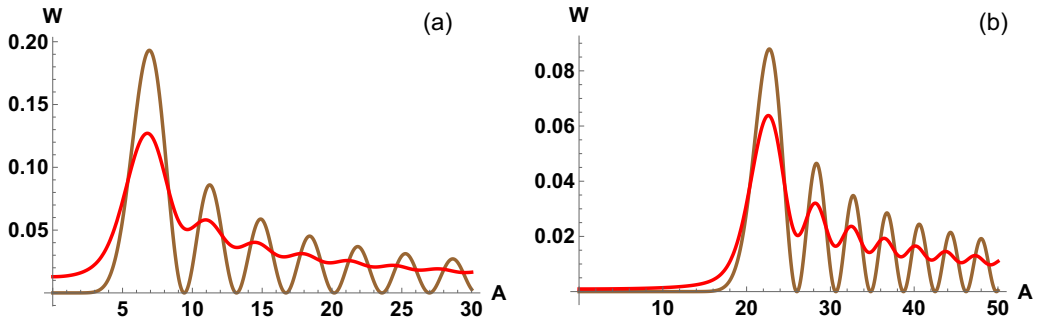

FIG. 1. Plot of W (in units of Δ^2/ω) as a function of A (in units of ω) for the approximation (4) (brown curve) and the exact formula (9) (red curve), with $\Gamma_2 = 5\omega/2\pi$ and (a) $\mathcal{E} = 5.5\omega$ and (b) $\mathcal{E} = 20.5\omega$.

II. ANALYSIS OF THE TRANSITION RATE

Consider the two-level system studied in [7] of a periodic driving on a qubit, with the Hamiltonian

$$\mathcal{H} = -\frac{1}{2}\begin{pmatrix} h(t) & \Delta \\ \Delta & -h(t) \end{pmatrix}, \tag{1}$$

where $h(t) = \mathcal{E} + \delta\mathcal{E}(t) + A\cos\omega t$ is the energy detuning (or bias) from an avoided crossing, modulated by the driving field. The term $\delta\mathcal{E}(t)$ describes classical noise and Δ is the energy gap between the two levels. The LZ transition rate was computed in perturbation theory in [7], with the result

$$W = \frac{\Delta^2}{2}\sum_{n=-\infty}^{\infty}\frac{\Gamma_2 J_n^2(x)}{(\mathcal{E}-\omega n)^2+\Gamma_2^2}, \quad x \equiv \frac{A}{\omega}, \tag{2}$$

where J_n is the Bessel function of the first kind. Note the symmetry property $W(-\mathcal{E}) = W(\mathcal{E})$. The parameter $\mathcal{E}$ is the energy bias and Γ_2 is the decoherence rate [3,7].[1]

The sum in Eq. (2) is usually evaluated numerically. However, attempts have been made to provide analytic approximations, as analytic formulas can reveal properties that are difficult to identify using numerical methods with generic parameters. In particular, in [7], and later on in [3,18], this sum was computed by assuming that the main contributions come from large-n terms, with the replacement

$$J_n(x) \approx a\,\mathrm{Ai}[a(n-x)], \quad a = (2/x)^{1/3}. \tag{3}$$

This approximation works well for a few oscillations, but then the two functions $J_n(x)$ and $a\,\mathrm{Ai}[a(n-x)]$ get out of phase.

The assumption that the main contributions come from large-n terms requires that $\mathcal{E} \gg \omega$ so that the sum is dominated by terms with $n \approx n_0$, where n_0 is the integer part of $\mathcal{E}/\omega$. In [7], the remaining sum was approximated by the heuristic formula

$$W_{\mathrm{app}} = \frac{\pi a^2\Delta^2}{2\omega}\mathrm{Im}[\cot(\pi\mu^*)]\mathrm{Ai}^2\left(\frac{a}{\omega}(\mathcal{E}-A)\right),$$
$$\mu \equiv \frac{1}{\omega}(\mathcal{E}+i\Gamma_2). \tag{4}$$

[1]If the relaxation time T_1 is taken into account, the upper level occupation probability can be calculated as in [3] (see Sec. 3.6 and Appendix B.4.2 therein). The resulting expression [Eq. (B.62) in [3]], the stationary solution of the rate equation, cannot be evaluated using our analytic formulas.

A numerical comparison shows that this formula approximates the sum (2) provided $\frac{\mathcal{E}}{\omega}$ is approximately equal to an integer much greater than 1 and $\Gamma_2 \ll 1$. A comparison between the original expression (2) and the approximation (4) is shown in Fig. 1. We see big deviations between W and W_{app} because in the figures $\mathcal{E}/\omega$ is not an integer. Since physically there is no reason for $\mathcal{E}/\omega$ to be an integer, generically W_{app} significantly deviates from the actual rate W. This evident deviation does not affect Fig. 4 in [7], as the fits with experimental data in that figure have been carried out by means of a numerical evaluation of the sum (2).

At large A, we can use the asymptotic formula for the Airy function, giving

$$W_{\mathrm{app}} \approx \frac{\Delta^2}{2x\omega}\mathrm{Im}[\cot(\pi\mu^*)]\left(1-\frac{\varepsilon}{x}\right)^{-1/2} \times \cos^2\left[\frac{2\sqrt{2}}{3}x\left(1-\frac{\varepsilon}{x}-\frac{\pi}{4}\right)\right]. \tag{5}$$

As will become clear in the following, this formula gives an incorrect asymptotic frequency.

The formula (4) reproduces some qualitative features of the actual rate W: In particular, W_{app} is very small for $A < \mathcal{E}$ (with $\mathcal{E} \gg \omega$), so transitions occur only for $A > O(\mathcal{E})$. The frequencies of oscillations are similar. However, it should be noted that minima and maxima are very different and also oscillations get out of phase after a few periods. Importantly, W_{app} has an infinite number of zeros as a function of x, but the exact W never vanishes for any finite Γ_2 and generic values of $\mathcal{E}$. The limit $\Gamma_2 \to 0$ will be discussed below.

We will now show that one can actually compute the sum (2) exactly and in closed form, using a summation formula derived in [19] (reviewed in Appendix A). Consider, in general, $\mu = \mu_1 + i\mu_2$. We first split

$$\sum_n \frac{J_n(x)^2}{(n-\mu_1)^2+\mu_2^2} = \frac{1}{2i\mu_2}\left(\sum_n \frac{J_n^2(x)}{n-\mu} - \sum_n \frac{J_n^2(x)}{n-\mu^*}\right). \tag{6}$$

Using the formula (A5), we thus find

$$\sum_n \frac{J_n(x)^2}{(n-\mu_1)^2+\mu_2^2} = -\frac{1}{2i\mu_2}\left(\frac{\pi}{\sin(\pi\mu)}J_\mu(x)J_{-\mu}(x) - \frac{\pi}{\sin(\pi\mu^*)}J_\mu^*(x)J_{-\mu}^*(x)\right) \tag{7}$$

or

$$\sum_n \frac{J_n(x)^2}{(n-\mu_1)^2+\mu_2^2} = -\frac{1}{\mu_2}\mathrm{Im}\left(\frac{\pi}{\sin(\pi\mu)}J_\mu(x)J_{-\mu}(x)\right), \tag{8}$$

where we used that $J_{\mu^*}(x) = J_\mu^*(x)$ for real x. Therefore,

$$W = -\frac{\Delta^2}{2\omega}\mathrm{Im}\left(\frac{\pi}{\sin(\pi\mu)}J_\mu(x)J_{-\mu}(x)\right). \tag{9}$$

A numerical check shows that indeed the formula (9) exactly reproduces the expression (2) given by the infinite sum.

Modulo an overall factor Δ^2/ω, W depends on three parameters ε, γ, and x, with

$$\varepsilon \equiv \frac{\mathcal{E}}{\omega}, \quad \gamma \equiv \frac{\Gamma_2}{\omega}, \quad x \equiv \frac{A}{\omega}.$$

We can set $\omega = 1$ and plot the rate W as a function of A for different values of $\mathcal{E}$ and Γ_2, as in Fig. 1. As noted above, the most notable difference is that the approximated transition rate (4) vanishes for specific values of x. This disagrees with the fact that the actual rate (2) and (9) does not vanish anywhere for generic values of Γ_2 and $\mathcal{E}$.

The transition rate (2) exhibits an infinite set of resonances created by the driving force, which appear at integer values of the detuning ε. All resonances are encapsulated in the exact formula (9). Indeed, at the special values $\mathrm{Re}(\mu) = n$, $n \in \mathbb{Z}$, we have

$$-\mathrm{Im}\left(\frac{\pi}{\sin(\pi\mu)}J_\mu(x)J_{-\mu}(x)\right) = (-1)^n\frac{\pi}{\sinh(\pi\gamma)}\mathrm{Re}[J_{n+i\gamma}(x)J_{-n-i\gamma}(x)]. \tag{10}$$

This shows that for integer ε the transition rate undergoes the expected enhancement at small γ,

$$-\mathrm{Im}\left(\frac{\pi}{\sin(\pi\mu)}J_\mu(x)J_{-\mu}(x)\right) \approx \frac{1}{\gamma}J_n^2(x) + O(\gamma), \tag{11}$$

a result that is also evident from the original formula (2), where the term $\mathcal{E} = \omega n$ dominates. This is in contrast with the behavior for generic (noninteger) values of ε, where the transition rate is proportional to γ.

Equation (11) shows that the height of the resonance peak is proportional to $J_n^2(x)$ and is therefore a function of the amplitude $A = x\omega$. For special values of the amplitude where the $J_n(x)$ has a zero, the peak at the detuning value $\varepsilon = \mathrm{Re}(\mu) = n$ disappears, but other peaks with $\varepsilon = n'$ (where $n' \neq n$) remain. Since the Bessel function possesses an infinite number of zeros, it is apparent that there are infinite special values of amplitude where the peak at any given detuning $\varepsilon = n$ is suppressed.

Equation (11) also clarifies that the transition rate may have zeros under two conditions: $\gamma \to 0$ and integer ε. In these cases, the zeros of the (rescaled) transition rate γW coincide with the zeros of the Bessel function $J_n(x)$.

A simple formula for W can also be given for large x, where we have the well-known Bessel asymptotics [20]

$$J_\mu(x) \approx \frac{\sqrt{2}}{\sqrt{\pi x}}\cos\left(x - \mu\frac{\pi}{2} - \frac{\pi}{4}\right), \quad x \gg \max\{1, |\mu|^2\}. \tag{12}$$

Thus, for large x,

$$-\mathrm{Im}\left(\frac{\pi}{\sin(\pi\mu)}J_\mu(x)J_{-\mu}(x)\right) \approx -\frac{1}{x}\mathrm{Im}\left(\frac{\cos(\pi\mu)+\sin(2x)}{\sin(\pi\mu)}\right). \tag{13}$$

Computing the imaginary part, we find

$$-\mathrm{Im}\left(\frac{\pi}{\sin(\pi\mu)}J_\mu(x)J_{-\mu}(x)\right) \approx \frac{2}{x}\frac{\sinh(\pi\gamma)}{\cosh(2\pi\gamma)-\cos(2\pi\varepsilon)}[\cosh(\pi\gamma)+\cos(\pi\varepsilon)\sin(2x)]. \tag{14}$$

Thus

$$W_{\mathrm{asym}} = \frac{\Delta^2}{x\omega}\frac{\sinh(\pi\gamma)}{\cosh(2\pi\gamma)-\cos(2\pi\varepsilon)}[\cosh(\pi\gamma) + \cos(\pi\varepsilon)\sin(2x)], \tag{15}$$

which is clearly different from (4) and (5). This formula explicitly shows the correct asymptotic frequency of oscillations in the $x = A/\omega$ variable, given by the factor $\sin(2x)$, which therefore differs from the frequency in the old approximation (5). It also provides an explicit expression for the amplitude of oscillations, which can be read from the above formula. A comparison between the exact W and W_{asym} is shown in Fig. 2.

The minimum and maximum values of the transition rate at any oscillating period can also be read from (15),

$$W_{\mathrm{asym}}|_{\max} = \frac{\Delta^2}{2x\omega}\frac{\sinh(\pi\gamma)}{\cosh(\pi\gamma)-\cos(\pi\varepsilon)}, \quad W_{\mathrm{asym}}|_{\min} = \frac{\Delta^2}{2x\omega}\frac{\sinh(\pi\gamma)}{\cosh(\pi\gamma)+\cos(\pi\varepsilon)}, \tag{16}$$

where we assumed $\cos(\pi\varepsilon) > 0$. As $\cos(\pi\varepsilon)$ flips sign, all minima become maxima and vice versa.

The general formula (8) can be applied in many experimental setups involving harmonic periodic driving. Some examples will be discussed below. The asymptotic formula (15) reveals some remarkable features. To leading order in the asymptotic expansion in $1/x$, the oscillations in the x variable are multiplied by $\cos(\pi\varepsilon)$, so they vanish for the special values of ε,

$$\varepsilon = n + \tfrac{1}{2}, \quad n \in \mathbb{Z},$$

giving

$$\frac{2}{x}\frac{\sinh(\pi\gamma)}{\cosh(2\pi\gamma)-\cos(2\pi\varepsilon)}[\cosh(\pi\gamma)+\cos(\pi\varepsilon)\sin(2x)] \to \frac{1}{x}\tanh(\pi\gamma). \tag{17}$$

For such special values of the detuning parameter $\mathcal{E} = \varepsilon\omega$ there is a significant suppression in the amplitude of oscillations in x, which becomes of $O(1/x^2)$ [the residual

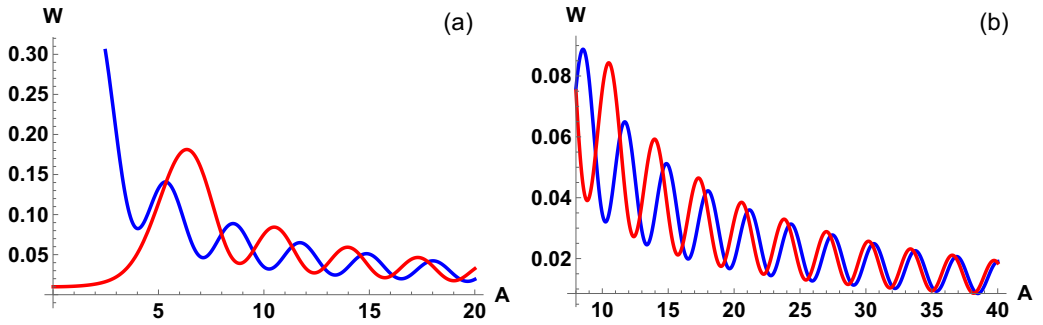

FIG. 2. At large amplitudes, the behavior of the transition rate is governed by the simple asymptotic behavior of the Bessel functions (red and blue curves correspond to W and $W_{\rm asym}$). Here $\varepsilon = 5$, $\gamma = 0.5$, and W is given in units of Δ^2/ω. (a) At small x, one can see a gap due to the well-known turning point of the Bessel functions around $x \sim |\mu|$ (i.e., $A \sim \mathcal{E}$). (b) When $x \gg |\mu|^2$, the asymptotic formula approaches the exact result.

oscillating $O(1/x^2)$ contribution originates from corrections to the asymptotic formula (12)]. This is shown in Fig. 3. This important property is only revealed after carrying out the exact summation over n, which may explain why it was overlooked in previous analyses.

Another noteworthy property of the formula (15) regards the γ dependence. For small γ and generic values of ε, the transition rate is $O(\gamma)$ due to the factor $\sinh(\pi\gamma)$. As discussed above, the expected resonances appear for integer ε, a property that is also manifest from the asymptotic formula

$$W_{\rm asym} \to \frac{\Delta^2}{2x\omega}\frac{1}{\sinh(\pi\gamma)}[\cosh(\pi\gamma) \pm \sin(2x)] \approx \frac{1}{\gamma}\frac{\Delta^2}{2\pi x\omega}[1 \pm \sin(2x)],$$

where the signs $\pm$ correspond to even and odd ε, respectively. Thus the transition rate becomes large, $O(1/\gamma)$. An exception arises for the special values of the amplitude where $\sin(2x) = \mp 1$, resulting in the suppression of the resonance peaks. These specific values of the amplitude $A = \omega x$ correspond to the asymptotic values of the zeros of $J_n(x)$, as previously discussed.

Note the marked change of behavior at special values of x. For generic x, the asymptotic transition rate is a periodic function of ε with period $\varepsilon = \varepsilon + 2n$. However, at the special values

$$x = \frac{n\pi}{2}, \quad n \in \mathbb{Z},$$

we have $\sin(2x) = 0$ and the period suddenly becomes $\varepsilon = \varepsilon + n$. It would be extremely interesting to experimentally test all these distinctive features.

Finally, it is also worth looking at the behavior of W at small amplitudes. Using[2] [21]

$$\frac{\pi}{\sin(\pi\mu)}J_\mu(x)J_{-\mu}(x) = \frac{1}{\mu}\left(1+\sum_{m=1}^{\infty}\frac{(2m)!}{2^{2m}(m!)^2}\frac{x^{2m}}{(\mu^2-1^2)(\mu^2-2^2)\cdots(\mu^2-m^2)}\right), \tag{18}$$

we find

$$W(x=0) = \frac{\Delta^2\gamma}{2\omega|\mu|^2}. \tag{19}$$

This formula is exact and encompasses the entire summation in (2). This nonvanishing value is clearly visible in Fig. 1(a) [where $W(x=0) \cong 0.013$]. This contrasts the exponentially small value inaccurately predicted by the old and commonly used approximation (4).

A number of studies extend the study of transitions to multiple energy levels and use W as a building block as the transition rate between a given pair of energy levels [22–24]. This introduces of course multiple energy bias parameters, one for each pair, and our evaluation applies directly to each W.

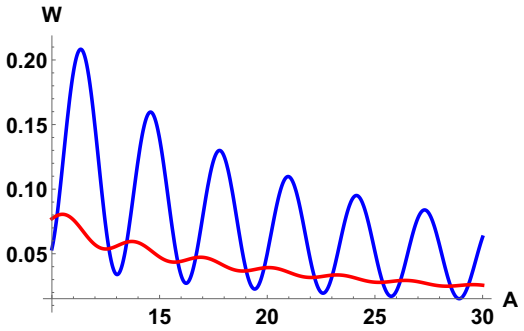

FIG. 3. Exact W given in (9) (in units of Δ^2/ω) as a function of A (in units of ω). The oscillations are strongly suppressed at half-integer values of the detuning parameter. Here $\gamma = 0.3$ and $\varepsilon = 5/2$ (red curve) and $\varepsilon = 1.2 \times 5/2$ (blue curve).

A. Upper-level occupation probability and Stückelberg phase

The formula (15) can also be written as

$$W_{\rm asym} = \frac{\Delta^2}{x\omega}b\left[a - \sin^2\left(x - \frac{\pi}{2}\varepsilon - \frac{\pi}{4}\right) - \sin^2\left(x + \frac{\pi}{2}\varepsilon - \frac{\pi}{4}\right)\right], \tag{20}$$

[2]The formula follows from an identity in [20].

with

$$b \equiv \frac{\sinh(\pi\gamma)}{\cosh(2\pi\gamma)-\cos(2\pi\varepsilon)}, \quad a \equiv 2\cosh^2\left(\frac{1}{2}\pi\gamma\right). \quad (21)$$

It should be noted that the oscillation frequency in the $x = A/\omega$ variable is equal to 2. This is in sharp contrast with the predicted asymptotic frequency of the approximation (4), where, for large A, it has the form (5) and predicts an incorrect frequency $\frac{4\sqrt{2}}{3} \neq 2$. As a consequence, at large x, the approximation (4) gets completely out of phase.

The above asymptotic behavior (20) can be compared with known results for the upper-level occupation probability, obtained within the adiabatic-impulse model, in the double-passage regime and in the fast passage limit $\Delta^2/A\omega \ll 1$ [3]. The upper-level occupation probability is the square of the absolute value of the probability amplitude and its time average is a sum of Lorentzian-shape k-photon resonances of higher analytical complexity than the transition rate [see Eq. (55) in [2]], but in the above limit, it is proportionally related to the transition rate, giving (see Appendix B4.4 in [3])

$$P_+^{\text{double}} \approx \frac{2\pi\Delta^2}{\omega A}\sin^2\left(x-\frac{\pi}{2}\varepsilon-\frac{\pi}{4}\right). \quad (22)$$

Thus we see that the asymptotic expression (20) corresponding to the exact transition rate reproduces the expected frequency and also the expected ε dependence, that is, it reproduces the Stückelberg phase.

B. Fourier transforms of the transition rate

We now compute the Fourier transforms of W in both variables $\mathcal{E}$ and A. The characteristic function of a Lorentzian is an exponential, that is,

$$\int_{-\infty}^{\infty}\frac{\lambda e^{ixt}}{\pi(\lambda^2+(x-x_0)^2)}\,dx = \exp(x_0 it-\lambda|t|).$$

We want to Fourier transform with regard to $\mathcal{E}$ both in itself and en route to the two-dimensional Fourier transform, discussed by other means in [9]. So we consider $\sum_{n\in\mathbb{Z}}\frac{J_n(x)^2\Gamma_2}{(\mathcal{E}-n\omega)^2+\Gamma_2^2}$ and instead of using (9) and then the transform, we carry out the term-by-term transform (the dominated convergence theorem allows us to exchange integration and summation) and then

$$\begin{aligned}\hat{W}(k_\mathcal{E},x) &= \frac{\Delta^2}{2}\sum_{n\in\mathbb{Z}}\int_{-\infty}^{\infty}\frac{J_n(x)^2\Gamma_2\,e^{-i\mathcal{E}k_\mathcal{E}}}{(\mathcal{E}-n\omega)^2+\Gamma_2^2}\,d\mathcal{E}\\ &= \frac{\pi\Delta^2}{2}\sum_{n\in\mathbb{Z}}J_n(x)^2\exp(-n\omega i k_\mathcal{E}-\Gamma_2|k_\mathcal{E}|). \quad (23)\end{aligned}$$

Notice that $k_\mathcal{E}$ has the dimension of time. The summation can be carried out. Recall Graf's addition theorem [20]

$$\sum_{l\in\mathbb{Z}}t^l J_l(x)J_{l+m}(y)=\left(\frac{y-x/t}{y-xt}\right)^{n/2}J_m\left(\sqrt{x^2+y^2-xy\frac{t^2+1}{t}}\right).$$

It simplifies since $m=0$ in our case,

$$\hat{W}(k_\mathcal{E},x) = \frac{\pi\Delta^2}{2}\exp(-\Gamma_2|k_\mathcal{E}|)J_0(\sqrt{2x^2[1-\cos(\omega k_\mathcal{E})]}), \quad (24)$$

i.e.,

$$\hat{W}(k_\mathcal{E},x) = \frac{\pi\Delta^2}{2}\exp(-\Gamma_2|k_\mathcal{E}|)J_0(2x|\sin(\omega k_\mathcal{E}/2)|). \quad (25)$$

The formula shows that $\hat{W}(k_\mathcal{E},x)$ has an infinite number of zeros in the real x axes, given by the zeros of the Bessel function. The $\hat{W}(k_\mathcal{E},x)$ exhibits an oscillatory behavior, with an amplitude modulated by the exponential factor $\exp(-\Gamma_2|k_\mathcal{E}|)$. In particular, the formula (25) predicts the following oscillatory behavior at small x:

$$\hat{W}(k_\mathcal{E},x) \approx \frac{\pi\Delta^2}{2}\exp(-\Gamma_2|k_\mathcal{E}|)\left[1-x^2\sin^2\left(\frac{\omega k_\mathcal{E}}{2}\right)\right], \quad x \ll 1. \quad (26)$$

We can now look for the Fourier transform with regard to the x variable (the amplitude) using either (23) or (24) or both. The route (24) seems simpler since we only have to transform $J_0(\alpha x)$, where $\alpha := 2|\sin(\omega k_\mathcal{E}/2)|$, and we know that [25]

$$\int_{-\infty}^{\infty}J_n(x)e^{-ik_x x}dx = \frac{2(-i)^n T_n(k_x)}{\sqrt{1-k_x^2}} \quad \text{for } |k_x|<1,$$

where T_n is the first degree Chebyshev polynomial (which will not appear because $n=0$ above). Then

$$\begin{aligned}\tilde{\hat{W}}(k_\mathcal{E},k_x) &= \pi\Delta^2\frac{\exp(-\Gamma_2|k_\mathcal{E}|)}{\alpha\sqrt{1-k_x^2/\alpha^2}}\\ &= \pi\Delta^2\frac{\exp(-\Gamma_2|k_\mathcal{E}|)}{\sqrt{2[1-\cos(\omega k_\mathcal{E})]-k_x^2}}. \quad (27)\end{aligned}$$

Recalling that $x = A/\omega$, in terms of A this reads

$$\tilde{\hat{W}}(k_\mathcal{E},k_A) = \pi\Delta^2\frac{\exp(-\Gamma_2|k_\mathcal{E}|)}{\sqrt{\frac{4}{\omega^2}\sin^2(\frac{\omega k_\mathcal{E}}{2})-k_A^2}}. \quad (28)$$

This formula agrees with the double Fourier transform in $\mathcal{E}$ and A given in (15) in [9]. However, here we find a new closed formula (25) for the single Fourier transform in $\mathcal{E}$ [and below also for the Fourier transform in A, $\hat{W}(\mathcal{E},k_x)$].

Fourier transform in A

The other partial (one-dimensional) Fourier transform, with respect to the variable x, can also be evaluated. The function $J_\mu(x)J_{-\mu}(x)$ is even in x; therefore [26]

$$\begin{aligned}\hat{W}(\mathcal{E},k_x) &= \frac{\pi}{\sin\pi\mu}\int_{-\infty}^{\infty}J_\mu(x)J_{-\mu}(x)e^{ixk_x}dx\\ &= \frac{2\pi}{\sin\pi\mu}\int_0^{\infty}J_\mu(x)J_{-\mu}(x)\cos(k_x x)dx. \quad (29)\end{aligned}$$

Computing the integral, we find

$$\hat{W}(\mathcal{E},k_x) = \begin{cases}\frac{\pi}{\sin\pi\mu}P_{\mu-1/2}\left(\frac{k_x^2}{2}-1\right) & \text{for } 0\leqslant k_x\leqslant 2\\ 0 & \text{for } k_x<0 \text{ or } k_x>2,\end{cases} \quad (30)$$

where $P_{\mu-1/2}$ is the Legendre function. Thus the Fourier transform gives a compact support function: The Fourier transformed transition vanishes identically outside the interval $0<k_x<2$.

A version of the Paley-Wiener theorem guarantees precisely that the Fourier transform of a function which is the real restriction of a complex entire function is a function of compact support and vice versa. The Bessel function $J_\mu(z)$ is indeed an entire function.

III. FLUORESCENCE SPECTRA OF QUANTUM DOTS

An examination of the literature and reviews on Floquet physics, specifically quantum systems under external ac (harmonic) field modulation, which includes a large number of photoassisted processes, will reveal a plethora of expressions of the type on the left-hand side of Eq. (A1). In previous studies, this expression was invariably left in summation form and customarily analyzed only numerically [27]. A prominent example is the power spectrum of fluorescence in quantum dots.

We recall that the transition rate in a modulated system is given by the Fourier transform of the stationary two-time correlation function of the Hamiltonian expressed in the interaction picture. Therefore, it is given by the power spectral density of the probe operator evaluated in the unperturbed system. Absorptive transitions in the rotating-wave approximation can be written as [27]

$$S(\omega) = \frac{g_P^2}{4}\int_{-\infty}^{\infty} e^{i\omega t}\langle\hat{\sigma}_-(t)\hat{\sigma}_+(0)\rangle dt, \tag{31}$$

where g_P represents the strength of the probe and $\hat{\sigma}_\pm$ are qubit raising and lowering operators. For harmonic modulations, this leads to the multiphoton sideband spectrum

$$S(\omega) = \sum_{m=-\infty}^{\infty}\frac{g_P^2}{2}\frac{\Gamma_2 J_m^2(x)}{(\delta+m\Omega)^2+\Gamma_2^2}, \tag{32}$$

where $\delta \equiv \omega_0 - \omega$ is the detuning between the static qubit and the probe. Thus we find the same expression arising in the preceding section in the context of superconducting qubits. Indeed, this formula controls the power spectrum in a broad class of two-level systems with harmonic driving [27,28].

Let us now consider the setting of [14], studying InAs/GaAs quantum dots. The formula (32) reappears in the form of resolved sideband emission, due to surface acoustic waves (SAWs) [14]. Indeed, some of the results in [14] are formally equivalent to the previous LZSM results. We will first present the equivalent model and subsequently discuss the effect of adding an interaction term to the Hamiltonian. This leads to a distinct application of the formula (A1).

The quantum dot (QD) is modeled as a two-level system in [14], with electric dipole operator $\hat{d} = d\sigma_x$, and dynamics governed by the Hamiltonian

$$H = \frac{\hbar}{2}[\omega_0 + \chi\omega_s \sin(\omega_s t)]\sigma_z \tag{33}$$

and relaxation terms that cause the off-diagonal elements of the density matrix ρ to decay at a rate γ. The σ_i are Pauli matrices and the modulation index χ is a dimensionless parameter that expresses the amplitude in units of ω_s.

The fluorescence is proportional to the expectation value $\langle\hat{d(t)}\rangle = \mathrm{Tr}[\rho(t)\hat{d}]$. In the limit $\omega_s \gg 2\gamma$, where 2γ denotes the linewidth, we find the following power spectrum of the fluorescence [14]:

$$P[\omega] = \sum_{n=-\infty}^{\infty}\frac{J_n^2(\chi)}{\gamma^2+(\omega-\omega_0+n\omega_s)^2}. \tag{34}$$

Applying the summation formula (8), we find

$$P[\omega] = -\frac{1}{\gamma\omega_s}\mathrm{Im}\left(\frac{\pi}{\sin(\pi\nu)}J_\nu(\chi)J_{-\nu}(\chi)\right),$$
$$\nu = \frac{1}{\omega_s}(\omega-\omega_0+i\gamma). \tag{35}$$

For large χ, we can express this result in terms of trigonometric functions, as in (14), and read the frequency thereof. We get

$$P[\omega]_{\mathrm{asym}} = \frac{2}{\chi\gamma\omega_s}b\left[\cosh\left(\frac{\pi\gamma}{\omega_s}\right) + \cos\left(\frac{\pi}{\omega_s}(\omega-\omega_0)\right)\sin(2\chi)\right], \tag{36}$$

where now

$$b \equiv \frac{\sinh(\pi\gamma/\omega_s)}{\cosh(2\pi\gamma/\omega_s)-\cos[2\pi(\omega-\omega_0)/\omega_s]}. \tag{37}$$

The power spectrum is governed by the same formula as the transition rate in (15), with a reinterpretation of the parameters. Therefore, it exhibits similar features. It has an oscillating behavior in the parameter χ, but at the special frequencies

$$\omega - \omega_0 = \omega_s\left(n+\tfrac{1}{2}\right), \tag{38}$$

the oscillating behavior is suppressed by an additional factor $1/\chi$, as $\sin(2\chi)$ has a vanishing coefficient in this case. As a function of ω, the asymptotic power spectrum is periodic with period $2/\omega_s$, but the period becomes $1/\omega_s$ at the special values of $\chi = n\pi/2$ where $\sin(2\chi) = 0$. On the other hand, at the resonant frequencies $\omega - \omega_0 = -n\omega_s$, the power spectrum undergoes the expected enhancement.

The experimental values in [14] for the modulation index χ are in the range $\chi \approx 0$–2 [see Fig. 3(b) in [14]]. The driving frequency is $\omega_s/2\pi = \nu_s = 1.05$ GHz and the linewidth is 250 MHz. It is instructive to see the changes in the fluorescence spectrum for these typical experimental values as one varies the driving frequency. Consider a resonance peak arising at $\omega - \omega_0 = -n_0\omega_s$, for some integer n_0. Taking, for example, $n_0 = 1$, if the sum is approximated by keeping only the terms $n = n_0, n_0 \pm 1$, as compared to the exact formula, the power spectrum around this peak changes between 5% and 20%, with bigger differences for larger χ. On the other hand, one can also observe the suppression of oscillations in χ occurring at half integer values of $(\omega-\omega_0)/\omega_s$ [corresponding to the minima in Fig. 3(a) in [14]]. By setting, for example, $\omega - \omega_0 = -\frac{1}{2}\omega_s$, $\omega_s/2\pi = \nu_s = 1.05$ GHz, then the oscillations in the interval $\chi = 1$–6 are significantly suppressed as compared with the oscillations at a generic value of $\omega - \omega_0$ (see Fig. 4). This illustrates the remarkable interference effect predicted by the exact analytic formula.

The study of quantum dots naturally prompts consideration of an area where the summation formula (A1) can have multiple applications, namely, cavity optomechanics [29]. For

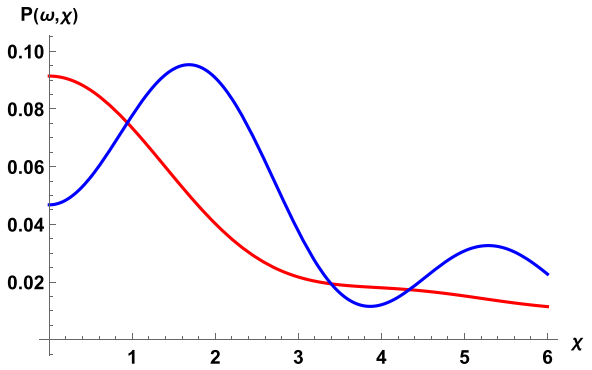

FIG. 4. Exact P given in (35) (in units of GHz^{-2}) as a function of the dimensionless modulation index χ. The oscillations are strongly suppressed at half-integer values of $(\omega-\omega_0)/\omega_s$. Here $\gamma = 0.25$ GHz and $\omega-\omega_0 = -\frac{1}{2}\omega_s$ (red curve) and $\omega-\omega_0 = -0.7\omega_s$ (blue curve).

example, it is possible to have sideband cooling of a nanomechanical resonator with an embedded QD [30], which involves the quantized transfer of energy from a mechanical mode of the resonator to the applied optical field. This was studied with resonant spectroscopy in [14].

The coupling of the resonant laser to the two-level system is described by adding to the Hamiltonian an additional interaction term

$$H_{\rm int} = -dE_0\cos(\omega_L t)\sigma_x, \tag{39}$$

describing the dipole coupling of the QD to a laser field $E_0\cos(\omega_L t)$. In [14] the power spectrum of the fluorescence for weak excitations was found to be proportional to

$$P[\omega] = \sum_{\ell=-\infty}^{\infty}\left|\sum_{n=-\infty}^{\infty}\frac{J_{\ell+n}(\chi)J_n(\chi)}{\gamma - i(\omega_L-\omega_0+n\omega_s)}\right|^2 \times \delta(\omega-\omega_L+\ell\omega_s), \tag{40}$$

which can be obtained by calculating the time dependence of the atomic dipole moment in the steady state. This is of the form of a series of discrete lines at frequencies $\omega_\ell = \omega_L - \ell\omega_s$, spectrally separated from the excitation frequency by multiples of the SAW frequency. We now give an analytical evaluation of the strength of these lines.

The sum in (40) involves an alternative application of the summation formula (A1), where now α or β may be different from zero. This structure will be ubiquitous in cavity optomechanics. The emission frequencies differing from the excitation frequency corresponds to the transfer of mechanical energy to the light field.

Using (A2), we find

$$\sum_{n=-\infty}^{\infty}\frac{J_{\ell+n}(z)J_n(z)}{n+\mu} = \frac{\pi}{\sin(\pi\mu)}J_{\ell-\mu}(z)J_\mu(z), \quad \ell\geqslant 0$$
$$\sum_{n=-\infty}^{\infty}\frac{J_{\ell+n}(z)J_n(z)}{n+\mu} = (-1)^\ell\frac{\pi}{\sin(\pi\mu)}J_{\mu-\ell}(z)J_{-\mu}(z), \quad \ell<0. \tag{41}$$

Therefore, we find

$$P[\omega] = P_+[\omega] + P_-[\omega], \tag{42}$$

where P_+ and P_- refer to the contributions from positive and negative ℓ, respectively, and they describe the two sets of frequencies of the spectrum $\omega = \omega_s \mp \ell\omega_s$. Explicitly,

$$P_+[\omega] = \frac{1}{\omega_s^2}\left|\frac{\pi}{\sin(\pi\mu)}J_\mu(\chi)\right|^2\sum_{\ell=0}^{\infty}|J_{\ell-\mu}(\chi)|^2 \times \delta(\omega-\omega_L+\ell\omega_s), \tag{43}$$

$$P_-[\omega] = \frac{1}{\omega_s^2}\left|\frac{\pi}{\sin(\pi\mu)}J_{-\mu}(\chi)\right|^2\sum_{\ell=1}^{\infty}|J_{\ell+\mu}(\chi)|^2 \times \delta(\omega-\omega_L-\ell\omega_s), \tag{44}$$

$$\mu = \zeta + i\eta, \quad \zeta \equiv \frac{\omega_L-\omega_0}{\omega_s}, \quad \eta \equiv \frac{\gamma}{\omega_s}. \tag{45}$$

The $P_+[\omega]$ and $P_-[\omega]$ exhibit an oscillatory behavior in χ and in ζ.

For large χ, the Bessel functions can be replaced by their asymptotic expressions. Explicit formulas are given in Appendix B. One can characterize the detailed features of the power spectrum and read frequencies and amplitudes thereof in terms of the physical parameters. The power spectrum has different properties in the "even" sector $\omega = \omega_L - 2k\omega_s$ and in the "odd" sector $\omega = \omega_L - (2k+1)\omega_s$. In particular, for $\omega = \omega_L - 2k\omega_s$, $k\in\mathbb{Z}$, in the limit that the linewidth $\gamma\to 0$, the power spectrum takes the simple form

$$P[\omega]_{\rm even} = \frac{[\cos(2\pi\zeta)+\sin(2\chi)]^2}{\chi^2\omega_s^2\,\sin^2(\pi\zeta)}\sum_k\delta(\omega-\omega_L+2k\omega_s). \tag{46}$$

The poles at integer ζ correspond to resonance peaks in the complete formula with $\gamma\neq 0$ (see Appendix B). The height of the peak is proportional to $[1+\sin(2\chi)]^2/\chi^2$, exhibiting a $1/\chi^2$ decrease at large χ. Remarkably, for the special values

$$\chi = -\frac{\pi}{4}+\pi n, \quad n\in\mathbb{Z},$$

all resonance peaks in the detuning parameter ζ disappear [modulo $O(1/\chi^3)$ corrections]. On the other hand, at the same special values of χ, $P[\omega]_{\rm odd}$ becomes $O(1)$ instead of $O(1/\gamma^2)$ at the resonance peaks located at integer values of ζ.

Another feature is the fact that the power spectrum (46) identically vanishes at parameters satisfying $\sin(2\chi) = -\cos(2\pi\zeta)$ (more precisely, at these special values $P_{\rm even}[\omega]$ is strongly suppressed and becomes $O(1/\chi^3)$). Similar features are shared by $P_{\rm odd}[\omega]$. It should be possible to test these intriguing properties in a laboratory setting.

A. Power spectrum in other QD systems

The use of Eq. (A2) is also applicable to a host of fluorescence spectra. The power spectrum is usually left in summation form (see, for example, [15,16,31]). However, it is now possible to compute all the infinite sums and provide the corresponding analytical expressions. Just as in the earlier examples, the closed formulas reveal important aspects of the physics that become manifest after resummation.

1. Coherent scattered light and atomic inversion

The spectrum of light scattered by a two-level atom in an intense laser beam with amplitude modulated light was considered long ago and just a few years after foundational works such as [17,32]. Analytical expressions already appeared in [15], in summation form, of a type similar to Eq. (40).

Reference [15] studied analytically the fluorescence spectrum in an amplitude modulated field, composed of a strong resonant component of frequency ω_0 and two considerably weaker sidebands of frequencies $\omega_0 \pm \omega_1$. It was found that the spectrum is characterized by a central component, insensitive to the presence of the modulating fields, and a series of sidebands centered about the Rabi frequency Ω_0 of the resonant field. The sidebands are located at frequencies $\Omega_0 + \omega_1 n$ for $n \in \mathbb{Z}$.

For the steady-state solution $\langle\sigma_+(t)\rangle$ of the optical Bloch equations, the spectral distribution of the coherently scattered light is [15]

$$I_{\rm coh}(\omega) \approx \frac{\pi\gamma^2}{8} \sum_{k=-\infty}^{\infty} Y_k Y_k^* \delta(\omega - \omega_L + k\omega_1),$$

where

$$Y_k \equiv \sum_{m=-\infty}^{\infty} J_m\left(\frac{a\Omega_0}{\omega_1}\right)\left(\frac{J_{m-k}\left(\frac{a\Omega_0}{\omega_1}\right)}{\frac{3}{4}\gamma - i(\Omega_0 + m\omega_1)} - \frac{J_{m+k}\left(\frac{a\Omega_0}{\omega_1}\right)}{\frac{3}{4}\gamma + i(\Omega_0 + m\omega_1)}\right). \tag{47}$$

Using (A2), we obtain

$$Y_k = \frac{i\pi}{\omega_1}\left((-1)^k \frac{J_{-\rho}J_{k+\rho}}{\sin(\pi\rho)} + \frac{J_{\rho^*}J_{k-\rho^*}}{\sin(\pi\rho^*)}\right) \quad \text{for } k \geqslant 0,$$

$$Y_k = \frac{i\pi}{\omega_1}\left(\frac{J_{\rho}J_{-k-\rho}}{\sin(\pi\rho)} + (-1)^k \frac{J_{-\rho^*}J_{-k+\rho^*}}{\sin(\pi\rho^*)}\right) \quad \text{for } k \leqslant 0,$$

where

$$\rho \equiv \frac{\Omega_0}{\omega_1} + i\frac{3\gamma}{4\omega_1}. \tag{48}$$

Therefore,

$$I_{\rm coh}(\omega) \approx \frac{\pi^3\gamma^2}{8\omega_1^2}\left(\sum_{k=0}^{\infty} a_k \delta(\omega - \omega_L + k\omega_1) + \sum_{k=-\infty}^{-1} b_k \delta(\omega - \omega_L + k\omega_1)\right),$$

with

$$a_k = \left|(-1)^k \frac{J_{-\rho}J_{k+\rho}}{\sin(\pi\rho)} + \frac{J_{\rho^*}J_{k-\rho^*}}{\sin(\pi\rho^*)}\right|^2,$$

$$b_k = \left|\frac{J_{\rho}J_{-k-\rho}}{\sin(\pi\rho)} + (-1)^k \frac{J_{-\rho^*}J_{-k+\rho^*}}{\sin(\pi\rho^*)}\right|^2.$$

Here the argument of all Bessel functions is $\frac{a\Omega_0}{\omega_1}$ as in the original expression (47). The formula now displays the explicit dependence of the spectral distribution in all physical parameters. It can be analyzed in the same form as done in previous examples.

2. Steady-state solutions: Atomic inversion

The steady-state atomic dipole moment $\langle\sigma_+(t)\rangle$ and inversion $\langle\sigma_z(t)\rangle$ are time dependent and contain oscillations for all the harmonics of the modulation frequency ω_1. The expectation value of $\langle\sigma_z(t)\rangle$ is equal to the difference between the upper-state and lower-state populations (atomic inversion) and γ denotes the spontaneous decay rate of the upper level [15].

We can obtain approximate solutions of the optical Bloch equations, valid for strong driving fields at resonance [$\Omega(t) \gg \gamma^2/16$]. The result is [15,33]

$$z(t) = \langle\sigma_z(t)\rangle = -\gamma\,\mathrm{Re}\left(\sum_{m,k=-\infty}^{\infty} \frac{J_{m-k}\left(\frac{a\Omega_0}{\omega_1}\right)J_m\left(\frac{a\Omega_0}{\omega_1}\right)\exp(-ik\omega_1 t)}{\frac{3}{4}\gamma - i(\Omega_0 + m\omega_1)}\right),$$

and $y(t) = -2i\langle\sigma_+(t)\rangle$ is given by a similar double-sum expression, with $-\gamma\,\mathrm{Re} \to \gamma\,\mathrm{Im}$ [15].

Thus, using (A2), we can now evaluate the atomic inversion term z_0 (corresponding to $k = 0$) and also any other subharmonic, for either positive or negative k. We obtain the following exact formulas for the harmonics:

$$z(t) = \sum_{k=-\infty}^{\infty} \beta_k e^{-ik\omega_1 t}, \tag{49}$$

$$\beta_k = (-1)^k \frac{\pi\gamma}{\omega_1}\mathrm{Im}\left(\frac{J_{-\rho}J_{k+\rho}}{\sin(\pi\rho)}\right) \quad \text{for } k \geqslant 0,$$

$$\beta_k = \frac{\pi\gamma}{\omega_1}\,\mathrm{Im}\left(\frac{J_{\rho}J_{-k-\rho}}{\sin(\pi\rho)}\right) \quad \text{for } k < 0. \tag{50}$$

The harmonics satisfy the following recurrence relations, inherited from the familiar recurrence relations of the Bessel functions:

$$\beta_{k+1} + \beta_{k-1} = -\frac{2\omega_1(k+\rho)}{a\Omega_0}\beta_k, \quad k \neq 0. \tag{51}$$

B. Asymmetric quantum dots with bichromatic electromagnetic field

In [16] an asymmetric quantum dot with broken inversion symmetry along the z axis together with a bichromatic field was considered,

$$\mathbf{E}(t) = \mathbf{E}_1 \cos\omega_1 t + \mathbf{E}_2 \cos\omega_2 t, \tag{52}$$

with $\mathbf{E}_1 = (0, 0, E_1)$ and $\mathbf{E}_2 = (E_2, 0, 0)$. It was also assumed that the second frequency ω_2 was close to the electronic resonance frequency, while the first frequency ω_1 was far from resonance. The resonance condition is

$$\omega_0 \pm \omega_2 = n\omega_1, \tag{53}$$

and in [16] all modes except the resonant one are neglected. Therefore, the parameter n above, denoting the number of modes, will appear in the power spectrum below. Then

$$F_n = -(d_{12}E_2/2\hbar)J_n(\tilde{\omega}/\omega_1) \tag{54}$$

are the Rabi frequencies of the considered system and

$$\tilde{\omega} = \frac{E_1(d_{22} - d_{11})}{\hbar} \tag{55}$$

is the effective frequency, whereas $\varphi_n = \omega_0 \pm \omega_2 - n\omega_1$ is the resonance detuning. The amplitudes of the fields are E_1 and E_2 and $d_{11} = \langle 1|ez|1\rangle$, $d_{22} = \langle 2|ez|2\rangle$, and $d_{12} = d_{21} = \langle 1|ex|2\rangle$ are the matrix elements of the operator of the electric dipole moment along the z and x axes, with e the electron charge.

The problem in [16] is thus reduced to the effective two-level system driven by a monochromatic field with the combined frequency φ_n. For simplicity in the formulas, we also define $\Omega_n = \sqrt{\frac{\varphi_n^2}{4} + F_n^2}$. Finally, using the dressed-atom method to discuss resonant fluorescence, we find for the width of the transitions [16]

$$\Gamma_{11} = \frac{\gamma}{2}\left(1 + \frac{\varphi_n^2}{4\Omega_n^2}\right), \quad \Gamma_{12} = \frac{\gamma}{4}\left(3 - \frac{\varphi_n^2}{4\Omega_n^2}\right), \tag{56}$$

where γ denotes the spontaneous emission rate.

The resulting inelastic power spectrum is given in terms of an infinite set of Mollow triplets [17] ($x \equiv \tilde{\omega}/\omega_1$):

$$\begin{aligned} S_2(\omega) \sim \frac{d_{12}^2}{4\pi}\Bigg[&\left(1 - \Delta_S^2\right)\left(\frac{d_{12}E_2}{2\hbar\Omega_n}\right)^2 J_n^2(x) \sum_m \frac{J_m^2(x)\Gamma_{11}}{[\omega - (n-m)\omega_1 - \omega_2]^2 + \Gamma_{11}^2} \\ &+ \frac{1}{2}\frac{\left(1 - \varphi_n^2/4\Omega_n^2\right)^2}{\left(1 + \varphi_n^2/4\Omega_n^2\right)} \sum_m \Bigg(\frac{J_m^2(x)\Gamma_{12}}{[\omega - (n-m)\omega_1 - \omega_2 + 2\Omega_n]^2 + \Gamma_{12}^2} \\ &+ \frac{J_m^2(x)\Gamma_{12}}{[\omega - (n-m)\omega_1 - \omega_2 - 2\Omega_n]^2 + \Gamma_{12}^2}\Bigg)\Bigg]. \end{aligned} \tag{57}$$

The infinite sums can now be carried out using our summation formula (8), giving

$$\begin{aligned} S_2(\omega) \sim -\frac{d_{12}^2}{4\pi\omega_1}\Bigg[&\left(1 - \Delta_S^2\right)\left(\frac{d_{12}E_2}{2\hbar\Omega_n}\right)^2 J_n^2(x)\mathrm{Im}\left(\frac{\pi}{\sin(\pi\nu_1)} J_{\nu_1}(x)J_{-\nu_1}(x)\right) \\ &+ \frac{\left(1 - \varphi_n^2/4\Omega_n^2\right)^2}{2\left(1 + \varphi_n^2/4\Omega_n^2\right)}\mathrm{Im}\left(\frac{\pi}{\sin(\pi\nu_2)} J_{\nu_2}(x)J_{-\nu_2}(x) + \frac{\pi}{\sin(\pi\nu_3)} J_{\nu_3}(x)J_{-\nu_3}(x)\right)\Bigg], \end{aligned} \tag{58}$$

where the spectral parameters of the Bessel functions are

$$\begin{aligned} \nu_1 &= n + \frac{1}{\omega_1}(\omega_2 - \omega + i\Gamma_{11}), \\ \nu_2 &= n + \frac{1}{\omega_1}(\omega_2 - \omega - 2\Omega_n + i\Gamma_{12}), \\ \nu_3 &= n + \frac{1}{\omega_1}(\omega_2 - \omega + 2\Omega_n + i\Gamma_{12}). \end{aligned}$$

IV. CONCLUSION

Sideband multiphoton spectra similar to (2), (40), and (57) are ubiquitous in two-level systems with harmonic modulation. In this paper we provided exact formulas that compute the infinite sums, enabling exploration of different spectra across all parameter space.

In Sec. II we saw that the transition rate is an oscillating function of the driving field amplitude that never vanishes. At large amplitude the exact transition rate can be written in terms of trigonometric functions, providing simple expressions to test a number of features. In particular, one interesting feature is the suppression of these oscillations for half-integer values of the detuning.

As a function of the detuning parameter (represented by $\mathcal{E}$ in Sec. II), the transition rate exhibits the expected resonance peaks at integer $\mathcal{E}$. We also noticed a significant change of behavior when x is an integer multiple of $\pi/2$, where the shape of the spectrum is simplified and the period is halved. We have also analytically determined the minimum and maximum values for each period of oscillations in (16).

Analogous properties were identified in the absorption spectra of quantum dots in Sec. III, where we also considered coupling to a more general configuration of driving fields. This included either the addition of an extra field or the consideration of bichromatic fields. In these cases, the required summation formula appeared in a different form, exploiting other particular instances of the analytical expression (A2), beyond the one employed in Sec. II. In all cases, closed formulas for the various spectra were obtained, which displayed explicit dependence on all physical parameters. Clearly, it would be worthwhile to conduct experiments to test the properties predicted by the analytical formulas in superconducting qubits or quantum dot devices.

ACKNOWLEDGMENTS

We thank David Pérez-García and Sergio Valenzuela for useful comments. J.G.R. acknowledges financial support from Generalitat de Catalunya through Grant No. 2021-SGR-249 and MINECO Grant No. PID2019-105614GB-C21. M.T. acknowledges financial support from Universidad Complutense de Madrid through Grant No. FEI-EU-22-06 and Spanish Ministry of Science and Innovation through Grant No. PID2020-113523GB-I00. This work was financially supported by the Ministry of Economic Affairs and Digital Transformation of the Spanish Government through the QUANTUM ENIA project Quantum Spain, by the European

Union through the Recovery, Transformation and Resilience Plan, NextGenerationEU, within the framework of the Digital Spain 2026 Agenda.

APPENDIX A: SUMMATION FORMULA

The more general form of the summation formula, found in [19], is

$$\sum_{n=-\infty}^{\infty} \frac{(-1)^n J_{\alpha+\gamma n}(z) J_{\beta-\gamma n}(x)}{n+\mu} = \frac{\pi}{\sin(\pi\mu)} J_{\alpha-\gamma\mu}(x) J_{\beta+\gamma\mu}(x), \tag{A1}$$

where $\mu \in \mathbb{C}/\mathbb{Z}$; $\alpha, \beta, x \in \mathbb{C}$; $\gamma \in (0, 1]$; and $\mathrm{Re}(\alpha+\beta) > -1$. It is useful to explicitly quote the particular case where $\gamma = 1$, $\alpha = p$, and $\beta = q$ (with $p, q \in \mathbb{Z}$), since this case frequently arises in various fluorescence spectra. The formula takes the form

$$\sum_{n=-\infty}^{\infty} \frac{J_{n+p}(z) J_{n-q}(x)}{n+\mu} = (-1)^q \frac{\pi}{\sin(\pi\mu)} J_{p-\mu}(x) J_{q+\mu}(x), \tag{A2}$$

where we used $J_{-n}(x) = (-1)^n J_n(x)$ and convergence now requires $p + q > -1$.

Here we provide a simple proof in the case $\alpha = \beta = 0$ and $\gamma = 1$, referring to [19] for the general case. Interestingly, the product of two Bessel functions admits different integral representations [20] in terms of the integration of a single Bessel function and an additional simple trigonometric or hyperbolic function. One of these representations is of Nicholson type,

$$J_n(x) J_{-n}(x) = \frac{2}{\pi} \int_0^{\pi/2} J_0(2x\cos\theta) \cos(2n\theta) d\theta. \tag{A3}$$

The Bessel function in the integrand is now independent of the summation index. Therefore, the summation only involves the cos term. The simple nature of the formula and of its derivation lies in the fact that the result of the summation

$$\sum_{n=-\infty}^{\infty} \frac{(-1)^n \cos n\phi}{n+\mu} = \frac{\pi \cos\mu\phi}{\sin\pi\mu}, \tag{A4}$$

where $\phi \in [-\pi, \pi]$, which is satisfied in our case, does not modify the analytical form of the integrand, because the right-hand side of (A4) also has a cosine with the integration variable. Therefore, the resulting integral expression after the summation has the same integral representation of the product of two Bessel functions.[3] Therefore,

$$\begin{aligned} \sum_{n=-\infty}^{\infty} \frac{J_n(x) J_n(x)}{n+\mu} &= \frac{2}{\sin\pi\mu} \int_0^{\pi/2} J_0(2x\cos\theta) \cos(2\mu\theta) d\theta \\ &= \frac{\pi J_\mu(x) J_{-\mu}(x)}{\sin\pi\mu}. \end{aligned} \tag{A5}$$

One of the first appearances, with a proof, of this formula is in [21]. The very first reference we could trace is actually [34]. This formula was rediscovered by Newberger [19], who also generalized it in the form (A1).

APPENDIX B: ASYMPTOTIC FORMULAS FOR THE FLUORESCENCE SPECTRUM

For large χ, we can again use the asymptotic formula for the Bessel function, giving

$$P[\omega] \approx P[\omega]_{\mathrm{asym}} = P[\omega]_{\mathrm{even}} + P_+[\omega]_{\mathrm{odd}} + P_-[\omega]_{\mathrm{odd}}, \tag{B1}$$

with

$$\begin{aligned} P[\omega]_{\mathrm{even}} &= \frac{4}{\chi^2\omega_s^2} \frac{\left|\cos\left(\chi - \mu\frac{\pi}{2} - \frac{\pi}{4}\right)\right|^2 \left|\cos\left(\chi + \mu\frac{\pi}{2} - \frac{\pi}{4}\right)\right|^2}{|\sin(\pi\mu)|^2} \sum_k \delta(\omega - \omega_L + 2k\omega_s), \\ P_+[\omega]_{\mathrm{odd}} &= \frac{4}{\chi^2\omega_s^2} \frac{\left|\cos\left(\chi - \mu\frac{\pi}{2} - \frac{\pi}{4}\right)\right|^2 \left|\sin\left(\chi + \mu\frac{\pi}{2} - \frac{\pi}{4}\right)\right|^2}{|\sin(\pi\mu)|^2} \sum_{k=0}^{\infty} \delta(\omega - \omega_L + (2k+1)\omega_s), \\ P_-[\omega]_{\mathrm{odd}} &= \frac{4}{\chi^2\omega_s^2} \frac{\left|\cos\left(\chi + \mu\frac{\pi}{2} - \frac{\pi}{4}\right)\right|^2 \left|\sin\left(\chi - \mu\frac{\pi}{2} - \frac{\pi}{4}\right)\right|^2}{|\sin(\pi\mu)|^2} \sum_{k=0}^{\infty} \delta(\omega - \omega_L - (2k+1)\omega_s). \end{aligned}$$

Computing the modulus, we find

$$\begin{aligned} P[\omega]_{\mathrm{even}} &= \frac{[\cosh(2\pi\eta)\cos(2\pi\zeta) + \sin(2\chi)]^2 + \sin^2(2\pi\zeta)\sinh^2(2\pi\eta)}{\chi^2\omega_s^2[\sin^2(\pi\zeta) + \sinh^2(\pi\eta)]} \sum_k \delta(\omega - \omega_L + 2k\omega_s), \\ P_+[\omega]_{\mathrm{odd}} &= \frac{[\cosh(2\pi\eta)\sin(2\pi\zeta) - \cos(2\chi)]^2 + \cos^2(2\pi\zeta)\sinh^2(2\pi\eta)}{\chi^2\omega_s^2[\sin^2(\pi\zeta) + \sinh^2(\pi\eta)]} \sum_{k=0}^{\infty} \delta(\omega - \omega_L + (2k+1)\omega_s), \\ P_-[\omega]_{\mathrm{odd}} &= \frac{[\cosh(2\pi\eta)\sin(2\pi\zeta) + \cos(2\chi)]^2 + \cos^2(2\pi\zeta)\sinh^2(2\pi\eta)}{\chi^2\omega_s^2[\sin^2(\pi\zeta) + \sinh^2(\pi\eta)]} \sum_{k=0}^{\infty} \delta(\omega - \omega_L - (2k+1)\omega_s). \end{aligned}$$

[3]The integral representation (A3) holds the same way for more general indices, including complex.

[1] P. Krantz, M. Kjaergaard, F. Yan, T. P. Orlando, S. Gustavsson, and W. D. Oliver, A quantum engineer's guide to superconducting qubits, Appl. Phys. Rev. **6**, 021318 (2019).

[2] S. N. Shevchenko, S. Ashhab, and F. Nori, Landau–Zener–Stückelberg interferometry, Phys. Rep. **492**, 1 (2010).

[3] O. V. Ivakhnenko, S. N. Shevchenko, and F. Nori, Nonadiabatic Landau–Zener–Stückelberg–Majorana transitions, dynamics, and interference, Phys. Rep. **995**, 1 (2023).

[4] F. Di Giacomo and E. E. Nikitin, The Majorana formula and the Landau–Zener–Stückelberg treatment of the avoided crossing problem, Phys. Usp. **48**, 515 (2005).

[5] P. O. Kofman, O. V. Ivakhnenko, S. N. Shevchenko, and F. Nori, Majorana's approach to nonadiabatic transitions validates the adiabatic-impulse approximation, Sci. Rep. **13**, 5053 (2023).

[6] E. Nikitin, Nonadiabatic transitions: What we learned from old masters and how much we owe them, Annu. Rev. Phys. Chem. **50**, 1 (1999).

[7] D. M. Berns, W. D. Oliver, S. O. Valenzuela, A. V. Shytov, K. K. Berggren, L. S. Levitov, and T. P. Orlando, Coherent quasiclassical dynamics of a persistent current qubit, Phys. Rev. Lett. **97**, 150502 (2006).

[8] W. D. Oliver, Y. Yu, J. C. Lee, K. K. Berggren, L. S. Levitov, and T. P. Orlando, Mach-Zehnder interferometry in a strongly driven superconducting qubit, Science **310**, 1653 (2005).

[9] M. S. Rudner, A. V. Shytov, L. S. Levitov, D. M. Berns, W. D. Oliver, S. O. Valenzuela, and T. P. Orlando, Quantum phase tomography of a strongly driven qubit, Phys. Rev. Lett. **101**, 190502 (2008).

[10] J. Li, M. Silveri, K. Kumar, J.-M. Pirkkalainen, A. Vepsäläinen, W. Chien, J. Tuorila, M. Sillanpää, P. Hakonen, E. Thuneberg *et al.*, Motional averaging in a superconducting qubit, Nat. Commun. **4**, 1420 (2013).

[11] Y. Gefen, E. Ben-Jacob, and A. O. Caldeira, Zener transitions in dissipative driven systems, Phys. Rev. B **36**, 2770 (1987).

[12] E. Shimshoni and Y. Gefen, Onset of dissipation in Zener dynamics: Relaxation versus dephasing, Ann. Phys. (NY) **210**, 16 (1991).

[13] Y. Gefen and D. J. Thouless, Zener transitions and energy dissipation in small driven systems, Phys. Rev. Lett. **59**, 1752 (1987).

[14] M. Metcalfe, S. M. Carr, A. Muller, G. S. Solomon, and J. Lawall, Resolved sideband emission of InAs/GaAs quantum dots strained by surface acoustic waves, Phys. Rev. Lett. **105**, 037401 (2010).

[15] B. Blind, P. R. Fontana, and P. Thomann, Resonance fluorescence spectrum of intense amplitude modulated laser light, J. Phys. B **13**, 2717 (1980).

[16] G. Y. Kryuchkyan, V. Shahnazaryan, O. V. Kibis, and I. A. Shelykh, Resonance fluorescence from an asymmetric quantum dot dressed by a bichromatic electromagnetic field, Phys. Rev. A **95**, 013834 (2017).

[17] B. Mollow, Power spectrum of light scattered by two-level systems, Phys. Rev. **188**, 1969 (1969).

[18] R. M. Otxoa, A. Chatterjee, S. N. Shevchenko, S. Barraud, F. Nori, and M. F. Gonzalez-Zalba, Quantum interference capacitor based on double-passage Landau-Zener-Stückelberg-Majorana interferometry, Phys. Rev. B **100**, 205425 (2019).

[19] B. S. Newberger, New sum rule for products of Bessel functions with application to plasma physics, J. Math. Phys. **23**, 1278 (1982).

[20] G. N. Watson, *A Treatise on the Theory of Bessel Functions* (Cambridge University Press, Cambridge, 1922), Vol. 2.

[21] L. S. Hall, W. Heckrotte, and T. Kammash, Ion cyclotron electrostatic instabilities, Phys. Rev. **139**, A1117 (1965).

[22] X. Wen and Y. Yu, Landau-Zener interference in multilevel superconducting flux qubits driven by large-amplitude fields, Phys. Rev. B **79**, 094529 (2009).

[23] M. P. Liul, A. I. Ryzhov, and S. N. Shevchenko, Interferometry of multi-level systems: rate-equation approach for a charge qudit, Eur. Phys. J.: Spec. Top. **232**, 3227 (2023).

[24] M. P. Liul and S. N. Shevchenko, Rate-equation approach for multi-level quantum systems, Low Temp. Phys. **49**, 96 (2023).

[25] H. O. Beća, An orthogonal set based on Bessel functions of the first kind, Publ. Elektrotehn. Fakult. Ser. Mat. Fiz. **695**, 85 (1980).

[26] I. S. Gradshteyn and I. M. Ryzhik, in *Tables of Integrals, Series, and Products*, 8th ed., edited by D. Zwillinger (Elsevier, Amsterdam, 2015), p. 726, Sec. 6.672, Eq. 2.

[27] M. P. Silveri, J. A. Tuorila, E. V. Thuneberg, and G. S. Paraoanu, Quantum systems under frequency modulation, Rep. Prog. Phys. **80**, 056002 (2017).

[28] M. P. Silveri, K. S. Kumar, J. Tuorila, J. Li, A. Vepsäläinen, E. V. Thuneberg, and G. S. Paraoanu, Stückelberg interference in a superconducting qubit under periodic latching modulation, New J. Phys. **17**, 043058 (2015).

[29] M. Aspelmeyer, T. J. Kippenberg, and F. Marquardt, Cavity optomechanics, Rev. Mod. Phys. **86**, 1391 (2014).

[30] I. Wilson-Rae, P. Zoller, and A. Imamoğlu, Laser cooling of a nanomechanical resonator mode to its quantum ground state, Phys. Rev. Lett. **92**, 075507 (2004).

[31] Z. Ficek, J. Seke, A. V. Soldatov, and G. Adam, Fluorescence spectrum of a two-level atom driven by a multiple modulated field, Phys. Rev. A **64**, 013813 (2001).

[32] C. Cohen-Tannoudji, in *Frontiers in Laser Spectroscopy*, edited by R. Balian, S. Haroche, and S. Liberman (North-Holland, Amsterdam, 1977), p. 3.

[33] P. Thomann, Optical resonances in a strong modulated laser beam, J. Phys. B **13**, 1111 (1980).

[34] H. K. Sen, Solar enhanced radiation and plasma oscillations, Phys. Rev. **88**, 816 (1952).